

Received: 14 September 2017 / Accepted: 22 November 2017 / Published online: 20 December 2017

*flat surfaces, contact, roughness,
FEM, 3D model*

Pawel MACIOLKA^{1*}
Jerzy JEDRZEJEWSKI¹

EVALUATION OF DIFFERENT APPROACHES TO 3D NUMERICAL MODEL DEVELOPMENT OF THE CONTACT ZONE BETWEEN ELEMENTARY ASPERITIES AND FLAT SURFACE

This paper presents two triaxial finite element (FE) models: a “full model” and a “quarter model”, representing the contact between the specimen’s rough surface and the ideally smooth and flat surface of the punch. Models have a contact zone that represents the topography of the real surface and has elastoplastic properties close to those of the real contact. The contact zone was entirely modelled on the basis of roughness measurements performed on a real milled specimen made of 5083 aluminium alloy. The development of the FE models, the stages in their refinement and the interlinking of the contact zone with the material of the specimen are described. The results of the computed deformations occurring during the specimen contact loading with the punch were compared with the experimental results. The possible causes of the observed deviations of the computer simulation results from the experimental ones were discussed. The models were used to analyse the effect of the specimen’s material properties, i.e. Young’s modulus, yield strength, compressive strength and material hardening, on the deformations in the contact. On this basis a procedure for predicting the parameters describing the contact characteristic in cases of changes in the properties of the subsurface zone is proposed.

1. INTRODUCTION

Designers of machines and their units commonly use numerical simulations to predict their properties in operating conditions using the available commercial CAE tools, such as Ansys, Abaqus and Patran. When modelling the connections between machine units and elements one often finds it difficult to model the stiffness of the contact between two rough surfaces. This stiffness is a major factor affecting the static and dynamic characteristics of machinery. The correctness and validity of its computational models is particularly critical when joints with a very small contact surface, occurring, for example, between the jugged object and the locators are to be numerically optimized [1,2]. Then the precision of locating and jugging machine parts, including frames and workpieces, can have a significant effect on the operational errors of the machines and in the case

¹ Wroclaw University of Science and Technology, Department of Machine Tools and Mechanical Technologies, Wroclaw, Poland

* E-mail: pawel.maciolka@pwr.edu.pl
DOI: 10.5604/01.3001.0010.7004

of machine tools, on the machining process errors. One of the causes of location errors are the deformations in the subsurface zone of the contacting machine elements, produced by the loads occurring during their assembly or fixing and operation.

The contact occurs each time when two surfaces are brought together and therefore methods of identifying and designing contact properties rank high in engineering practice [3]. Particularly suitable for this purpose are numerical statistical models [4,5] or deterministic models [6] for calculating the real surface area of contacts and consequently, their stiffness. Information on the actual surfaces being in contact is essential for reproducing the phenomena taking place in a contact joint. Statistical models and models based on fractals [7] require data on selected roughness parameters of the surfaces being in contact. Deterministic models require a matrix of the rough surface topography, which can be numerically generated or measured in the case of a real surface. There are many ways of generating rough surfaces, e.g., the Monte Carlo method [8], the autocorrelation function using the fast Fourier Transform (FFT) algorithm [9], and the fractal approach [10]. In FE models the topographies of the contacting surfaces are often represented by an arbitrary contact zone having properties as close as possible to those of the real contact. The models can be described using: springs with nonlinear characteristics [11], topographies generated numerically on the basis of the previously measured roughness parameters [12], or measurements of the topographies of real surfaces [13,14].

This paper is devoted to the last of the contact zone modelling methods. This creates the best chance of correct reproduction of the contact properties since the input data is directly derived from the real surface measurements.

2. 3D MODEL CONCEPT

The adopted 3D numerical model concept is intended for reproducing individual real surface asperities on the basis of surface topography measurements. The concept has been known for many years, but its practical degree of detail is low and depends on the computing power of the available computers. Since it was deemed crucial to reproduce individual asperities the adopted 3D models were to be verified experimentally. Besides the contact zone, the model concept includes the measuring stand components having a bearing on the accuracy and quality of identifying deformations. The full 3D model reproduces the components of the test stand developed by the authors and described in [15,16]. The following are modelled: a table, a milled rectangular specimen (made of 5083 aluminium alloy) whose top surface roughness is known, a steel punch ending in a short quadratic prism (ground and polished, with a 1 mm × 1 mm square cross section), and a contact zone together with a subsurface zone, constituting the principal part of the model (Fig. 1). In the geometric model of the specimen (a 50 mm × 50 mm quadratic prism) a small area was marked off and endowed with rough surface properties. The source of knowledge about the properties are the results of roughness measurements taken within a 4 mm × 4 mm area of the specimen by means of a CCILite TaylorHobson profilometer.

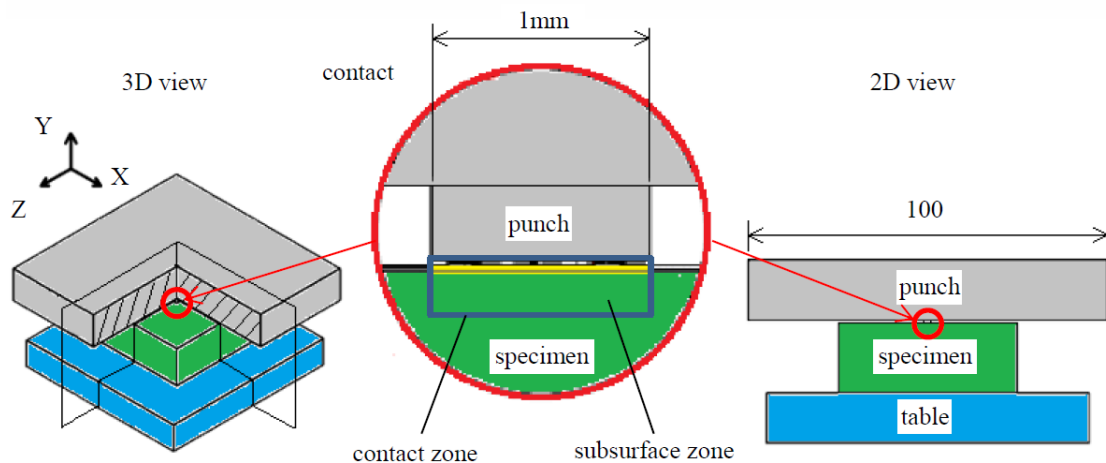


Fig. 1. Geometric model of contact joint

Parameters S_z (S_z – the maximum height of the surface) were determined from the measurements of the roughness of the milled specimen and the polished punch surface. A comparison of the roughness parameters S_z shows a large difference (more than one order of magnitude). Therefore it can be assumed that there is contact between the rough surface and the ideally smooth surface. Moreover, since the cross-sectional area of the punch is very small (1 square mm), whereby the waviness has been reduced from $5\ \mu\text{m}$ to less than $0.2\ \mu\text{m}$, the punch surface can be assumed to be ideally flat. On this basis a 3D FE model of the contact between the rough surface of the specimen and the ideally smooth and flat surface of the punch was created. The model represents a contact in which the punch is ideally stiff and devoid of any material properties. The profile of the rough surface was reproduced on the basis of the measurements performed using the profilometer and it was endowed with the material properties characterizing the whole specimen. The material properties were obtained from a compressive strength test carried out in accordance with Polish standard PN-H-04320:1957 “Static compressive test for metals”.

3. CONTACT ZONE MODEL

In the first computations the specimen’s top surface was modelled as ideally smooth with a marked small (slightly above $1\ \text{mm}^2$) area tied to a thin contact zone representing the roughness of the milled surface of the specimen (Fig. 2). The contact zone had to be so tied up with the specimen core material that it represented the properties of a real rough surface. The surface asperities were $12.5\ \mu\text{m}$ high. The thickness of the contact zone is variable and depends on solely the set of measurement data imported into the contact zone model. The import consisted in entering a cloud of points obtained from the profilometer, and forming a geometric solid (with its height varying consistently with the profilogram) from the points. The thickness of the contact zone was assumed to be equal to the maximum height of the asperities in the considered area of the specimen’s surface.

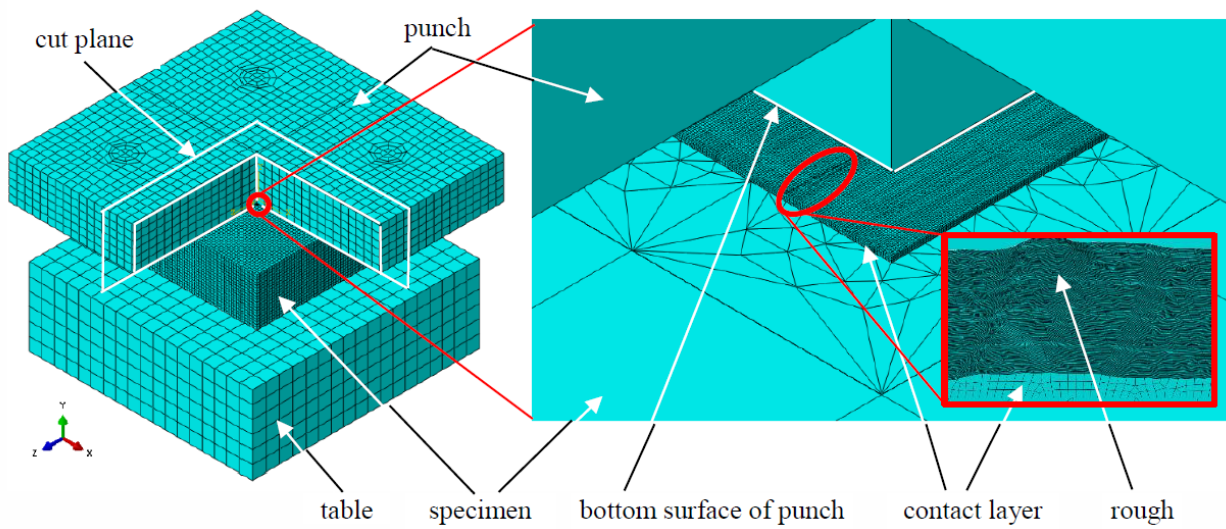


Fig. 2. Location of contact zone between smooth surface of punch and smooth surface of specimen core

Figure 3 shows a 3D image of the roughness of the milled specimen made of the aluminium alloy, measured after the first loading, in the specimen's central region within a 3.46×3.46 mm area (Fig. 3a). The location of the 1×1 mm area selected for contact zone modelling corresponds to the location and dimensions of the punch in the model (Fig. 3b). The roughness profiles in cross sections X-X and Y-Y are shown in Fig. 3c and Fig. 3d.

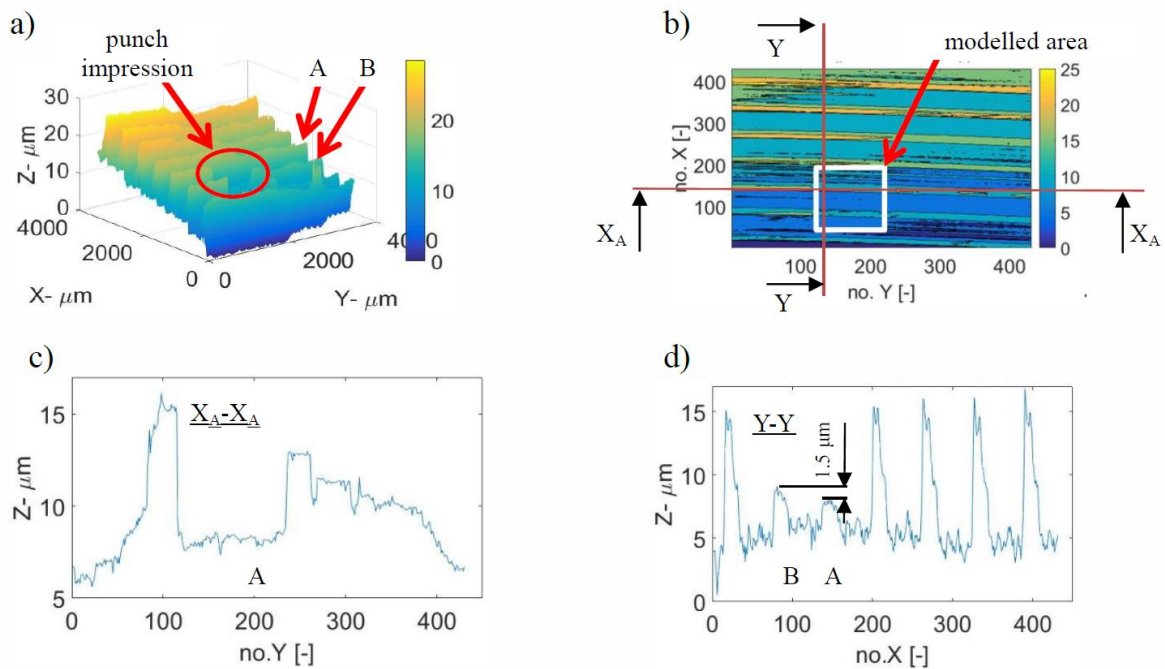


Fig. 3. Surface roughness of specimen made of 5083 aluminium alloy: a) punch impression, b) location of area selected for contact zone modelling, c) profile of asperities A in cross section X-X, d) profile in cross section Y-Y

In order to tie up the contact zone with the specimen's surface (the two surfaces differ in the number of nodes and the type of finite elements) "tie constraints" were defined in Abaqus. Thanks to this the displacements caused by stresses are transferred from the punch via the contact zone into the subsurface zone (Fig. 4). The values of the displacements are closely connected with the properties of the specimen material (5083 aluminium alloy). For the needs of the model the aluminium alloy's properties were determined through compressive strength tests. The tests was carried out in accordance with Polish Standard PN-H-04320:1957 in an Instron5982 strength testing machine and the results were analytically processed and verified using the available BlueHill3 computer program.

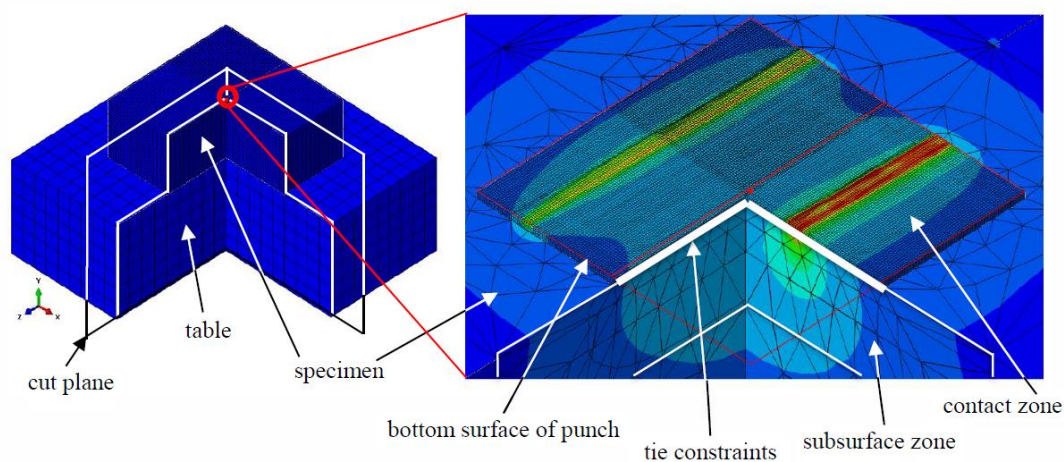


Fig. 4. Displacements observed during specimen loading, indicating that contact zone and specimen surface have been effectively tied together

Because of the small geometric dimensions of the contact zone (reproducing the shapes of the real roughness) it was necessary to use a very dense discretization grid with a maximum node spacing of 4-9 μm . The contact layer was modelled with 3D elements of the C3D8R type. If such a dense grid had been used in the other parts of the model, the computations would not have been completed within a reasonable time (a few hours). Therefore 3D elements, but with a considerably larger node spacing of 0.05-5 mm, were used to model the other model parts having simple geometric shapes, such as: the specimen, the table, the punch and the subsurface zone. In order to preserve the symmetry of the grid elements and taking into consideration the computing time, optimal discretization grids had to be sought. The criterion consisting in preserving the greatest symmetry of the grid elements was fulfilled by dividing the geometry of the 3D models so that during the automatic generation of the grid the Abaqus program arranged nodes symmetrically. In addition, areas of insignificant values were distinguished from significant areas on the isomaps of grid node stresses and displacements. Large elements were used in the former areas while small elements were used in the latter areas, whereby the accuracy of the stress and displacement isomaps was improved without increasing the computing time.

4. SELECTION OF MODEL GRID ELEMENTS AND MODEL REDUCTION

Besides the model presented above, which was called a “full model”, a simplified model, called a “quarter model” was created by cutting it out of the full model (Fig. 5). The main difference between the two models is that only ¼ of the contact zone used in the full model is loaded, but its properties do not exhibit symmetry as it is the case in the other parts of the model. The negative consequence of this can be some differences in the calculated displacements while the positive consequence can be a much shorter computing time than in the case of full model computations. The simplified model was further refined (Table 1) to reduce the computing time and the required computing power, i.e. the number of processors and the size of the memory.

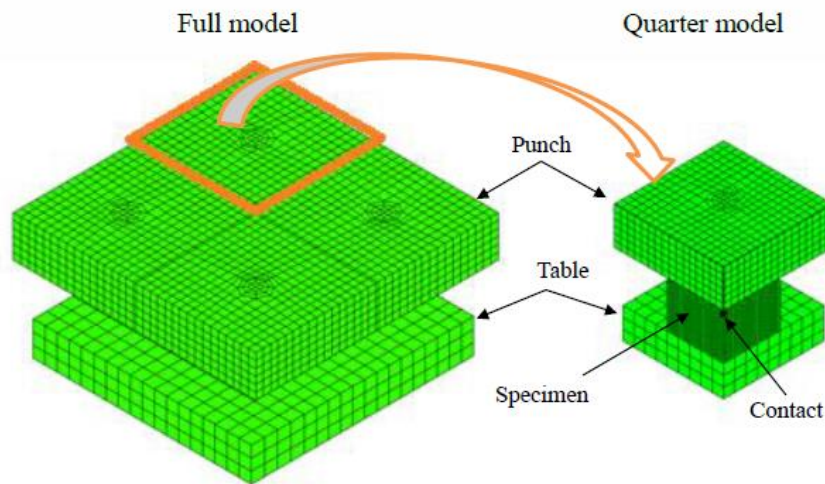


Fig. 5. Creation of quarter model

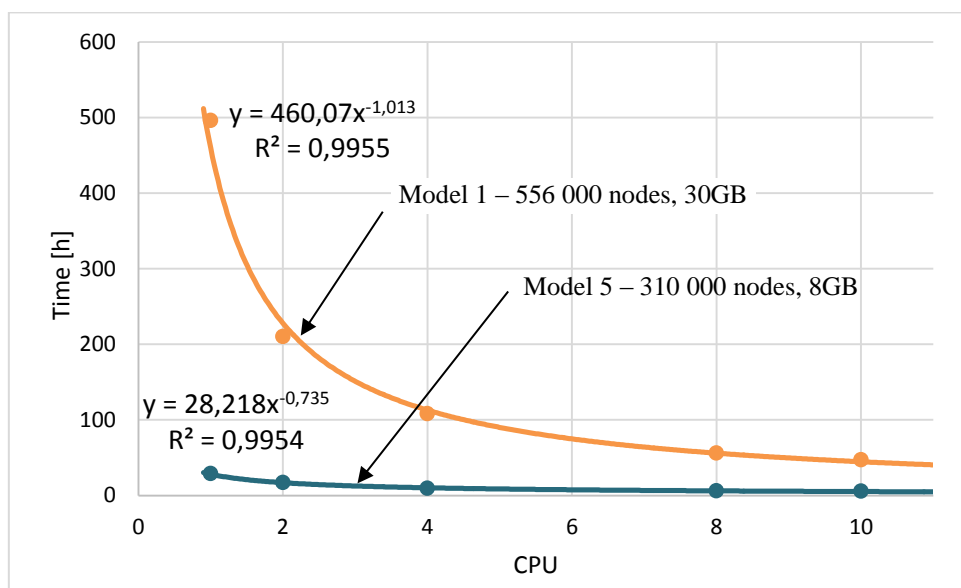
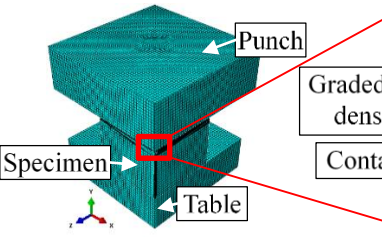
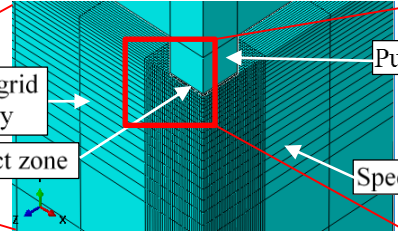
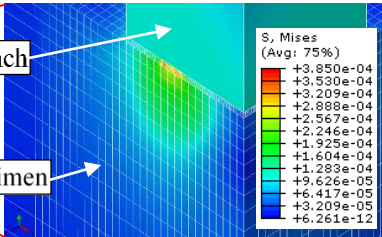
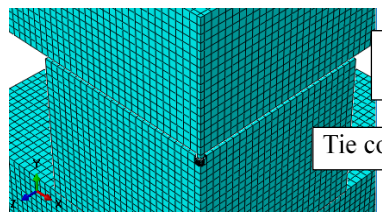
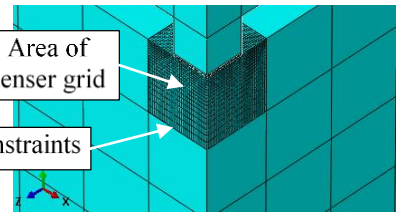
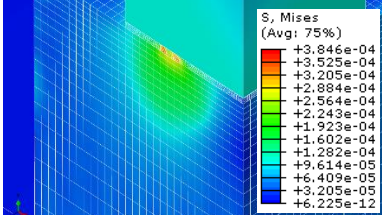

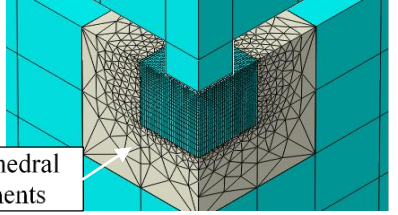
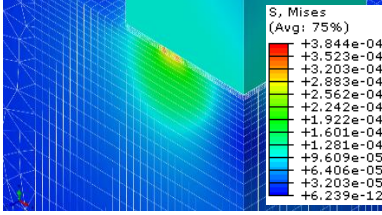
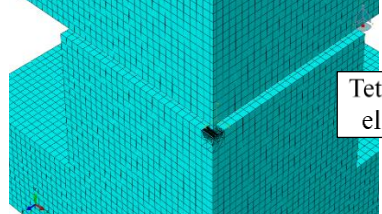
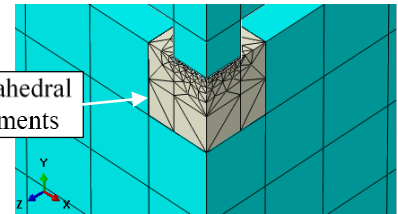
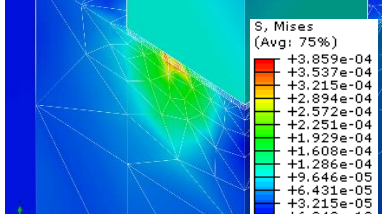
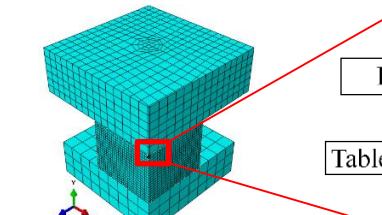
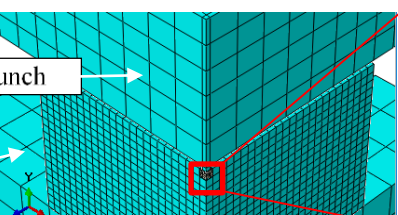
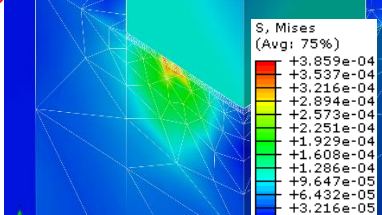


Fig. 6. Computing time versus amount of processors CPU for Quarter model

Figure 6 shows the dependence of computation time on the number of processors for the quadrant of the most and least time consuming model (No. 1 and 5) in Table 1. The data approximation by exponential function gives a good result ($R^2 = 0.995$). It can be concluded from the graph that by reducing the number of nodes in the model from 556k to 310k, you can reduce the computation time by 10 times. In this situation, some quality deterioration of stress or deformation isomaps may be expected.

Table 1. Steps in model refinement

View	Detail	Computations
1. Gradation of density of grid with cubic finite elements (30 GB of memory, Computing time 496h/1cpu,56h/8)		
 <p>Punch Specimen Table</p>	 <p>Graded grid density Contact zone</p>	 <p>S, Mises (Avg: 75%) +3.850e-04 +3.530e-04 +3.209e-04 +2.888e-04 +2.567e-04 +2.246e-04 +1.925e-04 +1.604e-04 +1.283e-04 +9.626e-05 +6.417e-05 +3.209e-05 +6.261e-12</p>
2. Reduction of denser grid area and introduction of tie constraints (13 GB of memory, 58/1cpu)		
	 <p>Area of denser grid Tie constraints</p>	 <p>S, Mises (Avg: 75%) +3.846e-04 +3.525e-04 +3.205e-04 +2.884e-04 +2.564e-04 +2.243e-04 +1.923e-04 +1.602e-04 +1.282e-04 +9.614e-05 +6.409e-05 +3.205e-05 +6.225e-12</p>
3. Introduction of tetrahedral elements in neighbourhood of contact zone (23 GB of memory, 371/1cpu)		
	 <p>Tetrahedral elements</p>	 <p>S, Mises (Avg: 75%) +3.844e-04 +3.523e-04 +3.203e-04 +2.883e-04 +2.562e-04 +2.242e-04 +1.922e-04 +1.601e-04 +1.281e-04 +9.609e-05 +6.406e-05 +3.203e-05 +6.239e-12</p>
4. Introduction of tetrahedral elements below contact zone (10 GB of memory, 38/2cpu)		
	 <p>Tetrahedral elements</p>	 <p>S, Mises (Avg: 75%) +3.859e-04 +3.537e-04 +3.215e-04 +2.894e-04 +2.572e-04 +2.251e-04 +1.929e-04 +1.608e-04 +1.286e-04 +9.646e-05 +6.431e-05 +3.215e-05 +6.243e-12</p>
5. Change of punch and table discretization (8 GB of memory, 29/1cpu, 6/8cpu)		
 <p>Punch Table</p>		 <p>S, Mises (Avg: 75%) +3.859e-04 +3.537e-04 +3.216e-04 +2.894e-04 +2.573e-04 +2.251e-04 +1.929e-04 +1.608e-04 +1.286e-04 +9.647e-05 +6.432e-05 +3.216e-05 +6.820e-11</p>

In step 1 the quarter model grid was automatically generated and the number of nodes near the contact was nonlinearly increased. In the case of this model, the time of computing a problem consisting in determining the full characteristic of displacements in the contact joint amounted to almost 500 hours for one processor at the required 30 GB of memory. The next computations were performed using two, eight and ten processors. As a result of the changes introduced into the model in steps 2, 3, 4 and 5 the computing time was reduced to 17 hours, and even to 6 hours when 8 processors were used at a memory requirement of 8 GB. But the changes introduced into the model in steps 1-5 had little effect on the strains which would occur during the loading and unloading of the contact. The refined model was described in Abaqus using 230 000 cubic and tetrahedral elements. The contact zone alone was modelled by 210 000 tetrahedral elements of the C3D8R type.

5. COMPUTATIONS OF CONTACT CHARACTERISTICS

The displacements and stresses in the contact joint were computed for the full cycle of loading-unloading the specimen with the roughness shown in Fig. 3. The isomaps of the stresses occurring in the contact between the rough specimen and the smooth steel punch for the full model and the quarter model are shown in Fig. 7. In both models the maximum von Mises stress in asperities area B amounted to 267 MPa. In both models this stress was accompanied by similar displacements of the nodes of the specimen contact zone grid. Slight differences were observed only in the size of the deformed area.

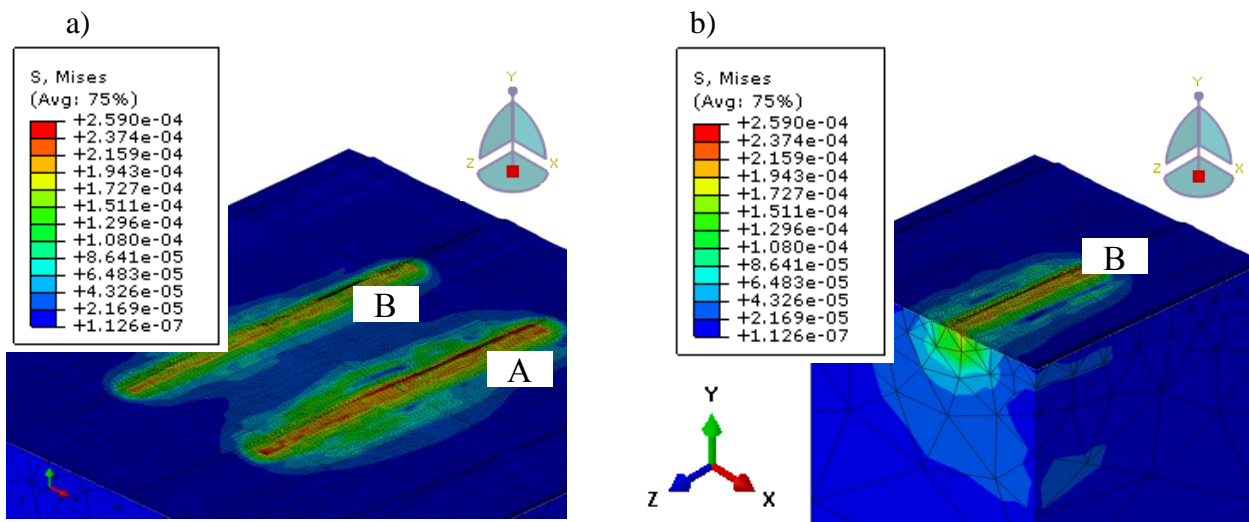


Fig. 7. Map of stresses in contact zone: a) full model – for contact load of 50 N, b) quarter model – for contact load of 12.5N (50/4 N).

The results of the computations of punch displacements relative to the specimen, induced by the elastic and plastic deformations caused by normal loads changing from 0 to 113 N, were compared (Fig. 8) with the experimental results (the reference) presented by the authors in an earlier publication [14].

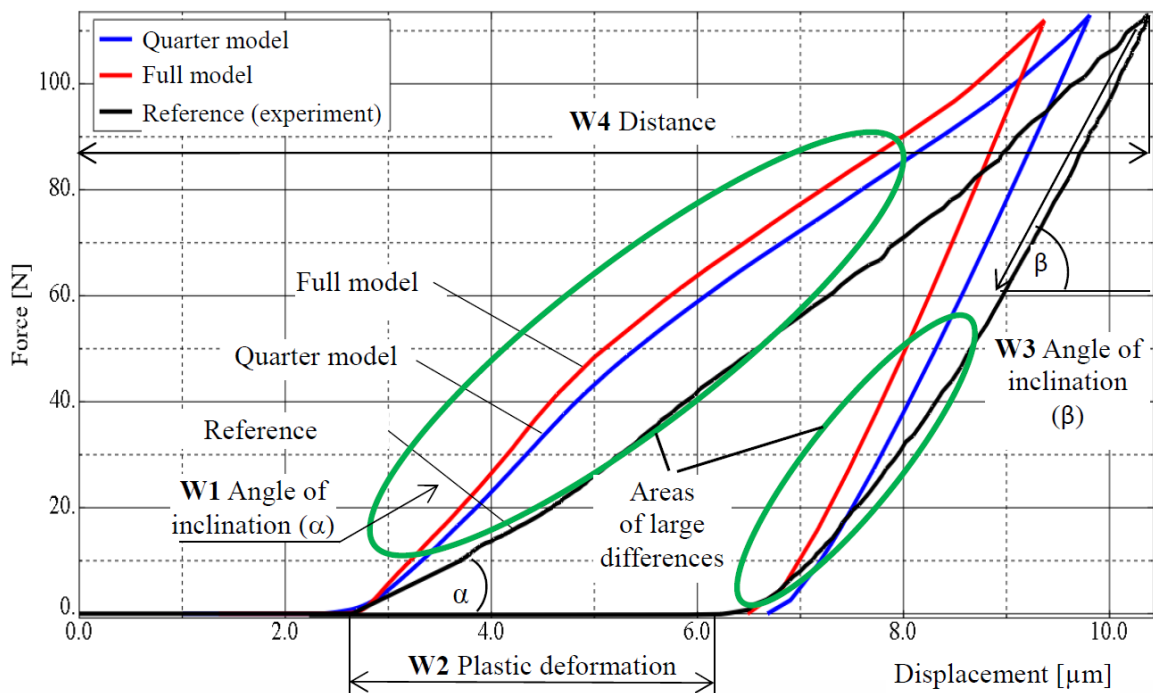


Fig. 8. Comparison of computed contact characteristics with experimental ones

It is apparent that the results obtained for the two models (the full model and the quarter model) differ in their character and values from the reference (the experimental curve), especially in the two areas marked in the figure. This applies to the shape of the load curve, the plastic deformation values and the angle of inclination of the characteristics in both the loading and unloading phase. Further in this paper an attempt is made to determine the causes of the deviations from the experimental characteristic. Some of the causes undoubtedly lied in the simplifying assumptions made in the quarter model, which provided an argument for using only the full model in further analyses. The model was used in several numerical simulations run to examine its response to changes in the material properties, initially only of the contact zone and ultimately of the subsurface zone together with the contact zone.

6. IMPACT OF SUBSURFACE ZONE MATERIAL PROPERTIES ON CONTACT CHARACTERISTICS – MODEL REFINEMENT

Improvement of the model described in sect. 4 showed that the differences between the computed contact deformation characteristic and the reference (experimental) one (Fig. 8) could not be significantly reduced by changing grid density and using different discretization elements. The effect of a change in the material properties of the subsurface zone, i.e. Young's modulus (E), yield strength (R) and compressive strength (R_c), on the FE model computation results was analysed. Such changes can be due to specimen surface hardening and permanent deformations during machining as well as during the first loading of the specimen. In the literature on the subject [16,17] it is reported that in the case

of aluminium alloy milling the residual stresses accompanying this strain hardening can reach deep into the material (as deep as 100-300 μm).

In order to describe the contact characteristics the following parameters p_i (shown graphically in Fig. 8) were used:

α – angle of inclination ($\alpha_{reference}=1.478$ rad, $W1=\alpha/\alpha_{reference}$)

Pd – plastic deformation ($Pd_{reference}=3.7$ μm, $W2=Pd/Pd_{reference}$)

β – angle of inclination ($\beta_{reference}=1.544$ rad, $W3=\beta/\beta_{reference}$)

D – distance ($D_{reference}=10.3$ μm, $W4=D/D_{reference}$).

Indices $W1-W4$, corresponding to parameters $p_i \in \{\alpha, Pd, \beta$ and $D\}$, are used to evaluate the agreement between the calculated material constants and the reference (experimental) values.

Impact factors $\eta_1-\eta_4$, defined in order to compare the intensity of the changes in indices $W1-W4$ and find out how any change in a selected physical property will change each of the four parameters $p_i \in \{\alpha, Pd, \beta$ and $D\}$ describing the contact characteristic, were determined on the basis of indices $W1-W4$. The impact factors were defined as a ratio of the increment in the value of each index (ΔWi) to the value of the change in the parameter ($\Delta E, \Delta Re$ or ΔRc) causing this increment.

Using Table 2 one can compare the intensities of the change in indices $W1-W4$, resulting from an increase in the value of E, Re or Rc . An increase in E results in an over three-fold larger change in $W4$ (an impact factor of 7.25) than, e.g., an increase in Re does (an impact factor of 1.88) and in an over several tens times larger change than in the case of an increase in Rc . The sign (-) indicates that the index value decreases.

Table 2. Factors of impact of change in subsurface zone physical properties on indices $W1-W4$

Physical properties of subsurface zone (SZ)	Impact factor ($\times 10^3$)			
	$\eta_1(W1)$	$\eta_2(W2)$	$\eta_3(W3)$	$\eta_4(W4)$
$E \uparrow$	1.54 \uparrow	0.00	0.32 \uparrow	-7.25 \downarrow
$Re \uparrow$	0.31 \uparrow	-5.25 \downarrow	0.04 \uparrow	-1.88 \downarrow
$Rc \uparrow$	0.03 \uparrow	-0.53 \downarrow	0.00	-0.19 \downarrow

In addition, it can be inferred from Table 2 which of the four parameters $p_i \in \{\alpha, Pd, \beta, D\}$ will change as a consequence of the change in value of each of the three properties E, Re , or Rc . And so the increasing of the E-modulus mainly decreases distance D at which the load direction changes (an impact factor of -7.25) and increases characteristic inclination α in the initial stage of the loading cycle (an impact factor of 1.54) and to a lesser degree inclination β in the final stage (an impact factor of 0.32). The value of permanent deformation Pd is mainly determined by yield strength Re , although as the latter is increased, also the vertex of the curve shifts (by distance D) in the same direction in which the E-modulus shifts, but to a several times smaller degree. The value of Rc determines mainly permanent deformations Pd , but its impact is by an order of magnitude lower than that of Re , whereas the E-modulus no longer has any impact here.

Moreover, knowing impact factors $\eta_1 - \eta_4$ one can predict (with no need for FE model computations) how any change in a selected physical property will affect each of the four parameters describing the contact characteristic. On the basis of indices W_i and impact factors η_i prognostic relations are formed according to the following scheme:

$$\Delta p_i = \eta_i \cdot P_{(i)reference} \cdot \Delta SZ_i \quad (1)$$

where: Δp_i – a change in predicted parameter α , Pd , β or D , η_i – and impact factor (Table 2), ΔSZ_i – the assumed change in the properties of the subsurface zone (E , Re or Rc).

For example, if one intends to increase the yield strength of the subsurface zone by $\Delta Re=20$ MPa, one should find an answer to the question by how many micrometres the permanent strain value will change (ΔPd). Substituting the data from Table 2 and the above reference values of parameter $Pd_{reference}$ one gets

$$\Delta Pd = -5.25 \cdot 10^{-3} \cdot 3.7 \cdot 20 = -0.388 \mu\text{m} \quad (2)$$

If one increases the yield strength by 20 MPa, one should expect the plastic strains to decrease by about 0.4 μm .

Simulations showed the need to take into account a small error in the specimen-punch parallelism, which occurred during measurements on the test stand. The evidence for the occurrence of the error is the difference in the depth of permanent deformation between asperities A and B, amounting to 1.5 μm (Fig. 4d). It was also found necessary to abandon the ideally stiff punch assumption and the simplifications concerning roughness reproduction: the density of the points modelling the shape of the asperity being deformed was increased in places as much as tenfold.

Figure 9 shows the end result (line 1) of building and refining the FE model. Now, when it includes the subsurface zone and with its increased strain hardening, is not encumbered with the specimen/punch parallelism error, takes into account punch compliance and faithfully reproduces the geometry of the asperities, the model as comprehensively as possible describes the phenomena which occurred during the measurements. The comparison with the experiment (line 3) indicates that the permanent deformations Pd yielded by the simulations are by over 0.5 μm larger than the measured ones. This can be due to the fact that the model as yet does not take into account the changes in the subsurface zone material properties (E , Re , Rc) which could have occurred as a result of milling the specimen and loading it during the experiment.

The research on the E-modulus of the subsurface zone for aluminium alloys conducted in other research centres shows it to be rather invariable along the depth of the subsurface zone despite the changes in hardness [18]. But the hardening of the subsurface zone can be accompanied by an increase in yield strength Re and in compressive strength Rc . According to Table 2, index W_2 , describing permanent deformations in this zone, depends mainly on these material properties. Line 2 in Fig. 9 shows the situation when the subsurface zone's yield strength Re and compressive strength Rc are by about 20 MPa greater than those of the specimen's core. According to the earlier prediction (formula 2), this would result in a decrease in the plastic deformations by about 0.4 μm . It is not possible to reduce the angle of inclination (β) of characteristic 2 since then it would be necessary

to decrease the E-modulus of the sample’s core or that of the subsurface zone. The more probable cause of the discrepancy between the angles in the case of characteristics 2 and 3 the specimen and the table, despite the use of a special underpressure connection.

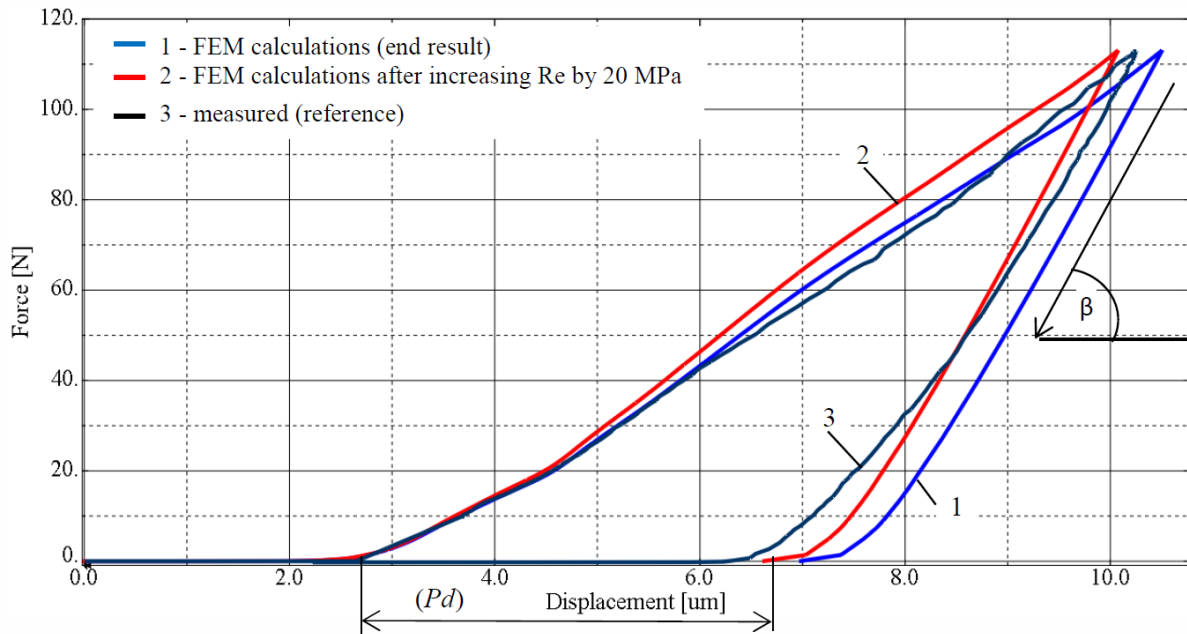


Fig. 9. Comparison of theoretical contact characteristics, calculated with and without changed subsurface zone material properties, with experimental curve

The material constants used to determine contact characteristics 1 and 2 shown in Fig. 9 are presented in Table 3.

Table 3. Material constant used to determine contact characteristics shown in Fig. 9

		$Re_{0,2}$, MPa	Rc , MPa	E , GPa	ν	Strain hardening
Characteristic 1	Specimen’s core	156	386	70	0.33	Nonlinear
	Subsurface zone and contact zone	156	386	70	0.33	Nonlinear
Characteristic 2	Specimen’s core	156	386	70	0.33	Nonlinear
	Subsurface zone and contact zone	176	406	70	0.33	Nonlinear

In the initial model the specimen and the contact zone were modelled. The thickness of the latter was equal to the height of the asperities. The contact zone and the specimen core were endowed with identical material properties. A subsurface zone (comprising the contact zone), initially having the same properties as the core and then changed (Table 3), was additionally introduced into the intermediate and final models. Increase of the Re and Rc parameters by 20 MPa in the Subsurface zone and contact zone

for Characteristic 2 of Table 3 results from the analysis. In the model, it was necessary to take into account the hardening of the subsurface zone. Therefore, the overall characteristics of aluminium alloy plastic hardening were lifted up to 20 MPa.

7. CONCLUSIONS

Using as an example the deformation of a specimen with two asperities the measures and computational analyses owing to which the phenomena taking place during the deformation of elementary asperities could be explored in detail have been discussed. A punch with a very small cross section (1 mm × 1 mm) had to be used in the investigations, which affected the design of the test stand. From the two considered FE models, i.e. the full model and the quarter model, the latter proved to be too imperfect and the principal analyses had to be carried out using only the full model. The feature of the two models was the import of a cloud of points obtained from a profilograph of the specimen's measured roughness and the generation of a spatial form of the asperities (the contact zone) on this basis. The same specimen was subjected to loading on the test stand whereby a contact characteristic was obtained. The characteristic was adopted as a standard (reference) to which the computational models should aspire. A procedure for predicting changes in the parameters describing the contact characteristic, caused by changes in the physical properties of the specimen material or that of the subsurface zone, has been developed in order to achieve better agreement between the calculation results and the measurement results. The procedure can be applied to other roughnesses and other materials.

The causes of the deviations of the computational models from the experimental characteristic have been identified and knowledge about the response of the models to changes in the material properties of the contact zone, the subsurface zone and the specimen core has been acquired.

The main findings of the article:

- In order to model the contact zone for elementary asperities, it was necessary to increase the plastic hardening of the contact zone by 20 MPa versus the plastic hardening of specimen's core obtained from the compression test. This was due to the hardening of the material which occurred during preparation of the specimen surface, i.e. during mechanical machining.
- Impact factors have been determined, which can be used to estimate the quantity of the impact of E , Re , and Rc changes on the load vs displacement characteristics.
- 300 μm subsurface zone and increased hardening material by 20 MPa led to the contact stiffness increase and plastic deformations decrease by 0.4 μm .
- The calculation time depends on the number of processors exponentially.
- An increase in the number of nodes in the model, leads to extension of calculation time but in return improves isomaps accuracy of stresses and displacements.
- Simplified Quarter Model has a negative influence on the results because he represent only $\frac{1}{2}$ part of one asperity while in the experiment were two and in addition unsymmetrical asperities.

ACKNOWLEDGEMENTS

The investigations have been carried out as part of the project WIPO INNOTECH-K1/INI/75/155671/NCBR/13 funded by the Polish National Centre for Research and Development (NCBiR). The measurements by means of the TalySurf CCILite (Taylor Hobson) profilometer were performed in the Laboratory of OptoMechatronics and Laser Technologies, Centre for Advanced Manufacturing Technologies, Wrocław University of Science and Technology. The computations were carried out in the Wrocław Centre for Networking and Supercomputing (<http://www.wcss.pl>) grant No.109.



REFERENCES

- [1] GROCHOWSKI M., 2010, *Model of mechatronic fixture with active error compensation*, Inżynieria Maszyn, 15/1-2, 67-79, (in Polish).
- [2] MACIOLKA P., JEDRZEJEWSKI J., 2008, *Modelling the behaviour of a contact layer between the workpiece and the locator*, Journal of Machine Engineering, 8/3, 42-53.
- [3] ITO Y., 2008, *Modular design for machine tools*, ISBN 10: 0071496602 / ISBN 13: 978007149660.
- [4] Xu Y., JACKSON R.L., MARGHITU D.B., 2014, *Statistical model of nearly complete elastic rough surface contact*, Int. J. Solids Struct., 51/5, 1075-1088.
- [5] GREENWOOD J.A., 2015, *On the almost-complete contact of elastic rough surfaces: The removal of tensile patches*, Int. J. Solids Struct., 56-57, 258-264.
- [6] MAKODONSKI Z., *A mathematical model of the contact between two real flat surfaces and of their deformations*, PhD thesis, Wrocław University of Technology, 1980, (in Polish).
- [7] GOERKE D., WILLNER K., 2008, *Normal contact of fractal surfaces-Experimental and numerical investigations*, Wear, 264, 589-598.
- [8] ZOU M., YU B., FENG Y. XU P., 2007, *A Monte Carlo method for simulating fractal surfaces*, Physica A, 386, 1, 176-186.
- [9] WU, J.J., 2000, *Simulation of rough surfaces with FFT*, Tribol. Int., 33/1, 47-58.
- [10] GANTI S., BHUSHAN B., 1995, *Generalized fractal analysis and its applications to engineering surfaces*, Wear, 180, 17-34.
- [11] BORA C.K., PLESHA M.E., CARPICK R.W., 2013, *A Numerical contact model based on real surface topography*, Tribology Letters, 50/3, 331-347.
- [12] ZHANG S., WANG W., ZHAO Z., 2014, *The effect of surface roughness characteristics on the elastic-plastic contact performance*, Tribol. Int., 79, 59-73.
- [13] WALTER C, ANTRETT T., 2009, *3D versus 2D finite element simulation of the effect of surface roughness on nanoindentation of hard coatings*, Surface Coatings Technology, 203, 3286-3290.
- [14] MACIOLKA P., JEDRZEJEWSKI J., GROCHOWSKI M., 2014, *A device for the experimental investigation of surface contact under load*, Journal of Machine Engineering, 14/3, 97-112.
- [15] MACIOLKA P., 2015. *Experimental investigation of flat surfaces in contact*, Journal of Machine Engineering, 15/2, 92-103.
- [16] DENKENA B., LEON L.D., 2009, *Milling induced residual stresses in structural parts out of forged aluminium alloys*, Int J Mach Mach Mater 4/4, 335-344.
- [17] HUANG X. SUN J., LI J., HAN X., XIONG Q., 2013, *An experimental investigation of residual stresses in high-speed end milling 7050-T7451 aluminium alloy*, Advances Mechanical Engineering, 7, DOI: 10.1155/2013/592659.
- [18] DRYZEK E., 2008, *Surface research of aluminium and aluminium alloys using annihilation positrons and complementary methods*, Habilitation thesis, Institute of Nuclear Physics, Polish Academy of Science, (in Polish).